High Step-Up Converter With Coupled-Inductor

Rong-Jong Wai, *Member, IEEE,* and Rou-Yong Duan

Abstract—In this study, a high step-up converter with a coupled-inductor is investigated. In the proposed strategy, a coupled inductor with a lower-voltage-rated switch is used for raising the voltage gain (whether the switch is turned on or turned off). Moreover, a passive regenerative snubber is utilized for absorbing the energy of stray inductance so that the switch duty cycle can be operated under a wide range, and the related voltage gain is higher than other coupled-inductor-based converters. In addition, all devices in this scheme also have voltage-clamped properties and their voltage stresses are relatively smaller than the output voltage. Thus, it can select low-voltage low-conduction-loss devices, and there are no reverse-recovery currents within the diodes in this circuit. Furthermore, the closed-loop control methodology is utilized in the proposed scheme to overcome the voltage drift problem of the power source under the load variations. As a result, the proposed converter topology can promote the voltage gain of a conventional boost converter with a single inductor, and deal with the problem of the leakage inductor and demagnetization of transformer for a coupled-inductor-based converter. Some experimental results via examples of a proton exchange membrane fuel cell (PEMFC) power source and a traditional battery are given to demonstrate the effectiveness of the proposed power conversion strategy.

Index Terms—Battery, converter, coupled inductor, fuel cell, passive regenerative snubber, proton exchange membrane, reverse recovery.

I. INTRODUCTION

RECENTLY, dc–dc converters with steep voltage ratio are usually required in many industrial applications. For example, the front-end stage for clean-energy sources, the dc back-up energy system for an uninterruptible power supply (UPS), high-intensity discharge lamps for automobile headlamps, and, finally, the telecommunications industry [1]–[3]. The conventional boost converters cannot provide such a high dc voltage gain, even for an extreme duty cycle. It also may result in serious reverse-recovery problems and increase the rating of all devices. As a result, the conversion efficiency is degraded and the electromagnetic interference (EMI) problem is severe under this situation [4]. In order to increase the conversion efficiency and voltage gain, many modified boost converter topologies have been investigated in the past decade [5]–[11].

R.-J. Wai is with the Department of Electrical Engineering, Yuan Ze University, Chung-Li, Taiwan, R.O.C. (e-mail: rjwai@saturn.yzu.edu.tw).

R.-Y. Duan is with the Department of Industrial Safety and Health, Hung Kuang University, Tai-Chung, Taiwan, R.O.C. (e-mail: ryduan2722@hotmail.com).

Although voltage-clamped techniques are manipulated in the converter design to overcome the severe reverse-recovery problem of the output diode in high-level voltage applications, there still exists overlarge switch voltage stresses and the voltage gain is limited by the turn-on time of the auxiliary switch [5], [6]. Silva *et al.* [7] presented a boost soft-single-switch converter, which has only one single active switch. It is able to operate with soft switching in a pulse-width-modulation (PWM) manner without high voltage and current stresses. Unfortunately, the voltage gain is limited below four in order to achieve the function of soft switching. In [8] and [9], coupled inductors were employed to provide a high step-up ratio and to reduce the switch voltage stress substantially, and the reverse-recovery problem of the output diode was also alleviated efficiently. In this case, the leakage energy of the coupled inductor is another problem as the switch was turned off. It will result in the high-voltage ripple across the switch due to the resonant phenomenon induced by the leakage current. In order to protect the switch devices, either a high-voltage-rated device with higher $R_{DS(on)}$ or a snubber circuit is usually adopted to deplete the leakage energy. In these ways, the power conversion efficiency will be degraded. Zhao and Lee [10] introduced a family of high-efficiency, high step-up dc–dc converters by only adding one additional diode and a small capacitor. It can recycle the leakage energy and alleviate the reverse-recovery problem. In this scheme, the magnetic core can be regarded as a flyback transformer and most of the energy was stored in the magnetic inductor. However, the leakage inductor of the coupled inductor and the parasitic capacitor of the output diode resonated after the switch was turned on, a proper snubber is necessary to reduce the output rectifier peak voltage. Moreover, the capacity of the magnetic core should be increased substantially when the demand of high output power is required.

Fuel cells are presently in the news because they appear to be one of the most efficient and effective solutions to the environmental pollution problem [12]–[18]. A fuel cell is an energy conversion device that produces electricity by electrochemically combining fuel (hydrogen) and oxidant (oxygen from the air) gases through electrodes across an ion conduction electrolyte. This process produces a much higher conversion efficiency than any conventional thermal–mechanical system because the system operates without combustion and extracts more electricity from the same amount of fuel. This system has the merits of high efficiency, energy security, reliability, is pollution-free, and has a quiet operation. Fuel cells have been known to science for more than 160 years and have recently become the subject of intense research and development. Until now, many demonstration projects have shown fuel cell systems to be feasible for portable power, transportation, utility power, and on-site power generation in a variety of building applications.
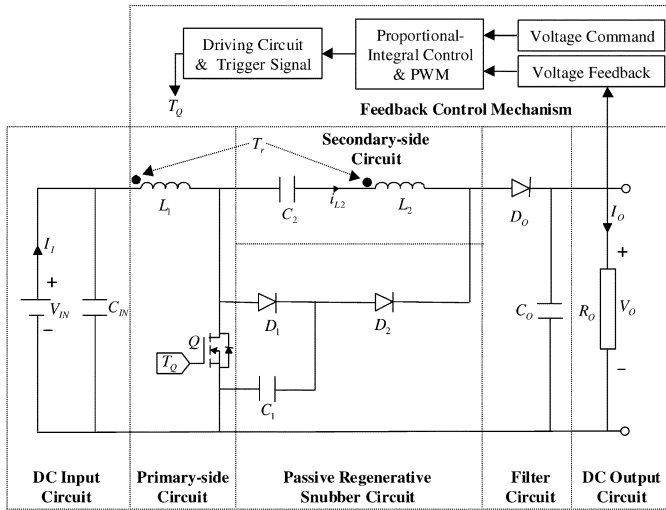
Fig. 1. System configuration of high step-up converter.

Fig. 2. Characteristic waveforms.

For portable power, a fuel cell with a fuel container can offer a higher energy density and more convenience than conventional battery systems. Moreover, portable power packs using fuel cells can be lighter and smaller in volume for an equivalent amount of energy. In transportation applications, fuel cells offer higher efficiency and better part-load performance than conventional engines. In stationary power applications, low emissions permit fuel cells to be located in high-power requirement areas where they can supplement the existing utility grid. Using fuel cells and hydrogen technology, electrical power can be delivered where and when required, cleanly, efficiently, and with sustainability. The greatest research interests throughout the world have focused on the proton exchange membrane (PEM) and solid oxide cell stacks. The PEMFC has promising characteristics: 1) the by-product waste is water, 2) low-temperature operation, and 3) they use a solid polymer as the electrolyte which reduces concerns related to construction, transportation, and safety issues [17]. Thus, it seems to be a good alternative source for distributed generation systems.

The aim of this study is to design a high-efficiency, high step-up converter with coupled-inductor to regulate a stable constant dc voltage. To achieve this goal, the manipulation of a coupled inductor with a lower-voltage-rated switch and a passive regenerative snubber circuit is adopted to promote the voltage gain. Moreover, the problems of the stray inductance and the diode reverse recovery in conventional boost converters also can be solved so that it can achieve the object of high-efficiency power conversion. In addition, the feedback control methodology is utilized in the proposed converter to overcome the voltage drift problem of the power source under the load variations. The remainder of this study is organized as follows. Section II presents the converter design and analyses in detail. Experimental results of a PEMFC system and a traditional battery are provided to validate the effectiveness of the proposed power conversion system in Section III. Conclusions are drawn in Section IV.
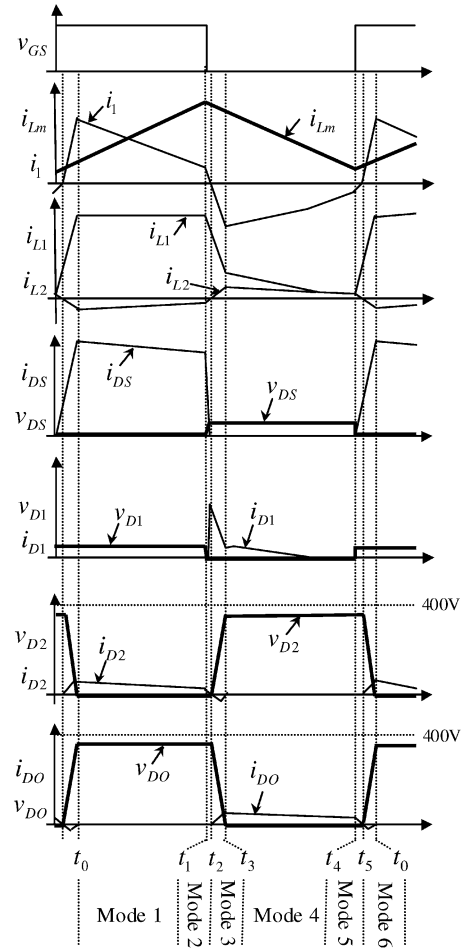
II. CONVERTER DESIGN AND ANALYSES

The system configuration of the proposed converter topology is depicted in Fig. 1, where it contains seven parts including a dc input circuit, a primary-side circuit, a secondary-side circuit, a passive regenerative snubber circuit, a filter circuit, a dc output circuit, and a feedback control mechanism. The major symbol representations are summarized as follows. V_{IN} and I_I denote dc input voltage and current, and C_{IN} is an input filter capacitor in the dc input circuit. L_1 and L_2 represent individual inductors in the primary and secondary sides of the coupled inductor (T_r), respectively. Q is a switch in the primary-side circuit and T_Q is a trigger signal in the feedback control mechanism. C_1, D_1, and D_2 denote a clamped capacitor, a clamped diode, and a rectifier diode in the passive regenerative snubber circuit. C_2 is a high-voltage capacitor in the secondary-side circuit. D_O and C_O are the output diode and the filter capacitor in the filter circuit. V_O and I_O describe output voltage and current; R_O is an output load.

The characteristic waveforms of the proposed high step-up converter are depicted in Fig. 2. Moreover, Fig. 3 illustrates the topological modes in one switching cycle and the detailed operation stages are described in Section II-A. The coupled inductor in Fig. 1 is modeled as an ideal transformer, a magnetizing inductor (L_m), and a leakage inductor (L_k) in Fig. 3. The turns

ratio (n) and coupling coefficient (k) of this ideal transformer are defined as

$$n = N_2/N_1 \qquad (1)$$
$$k = L_m/(L_k + L_m) \qquad (2)$$

where N_1 and N_2 are the winding turns in the primary and secondary sides, respectively. For simplicity, the dc input circuit in Fig. 1 is denoted as a constant voltage source V_S. The voltages across the switch, the primary and secondary winding of the ideal transformer, and the leakage inductor are denoted as $v_{\mathrm{DS}}, v_{Lm}, v_{L2}$, and v_{Lk}, respectively. Moreover, the primary current (i_{L1}) of the coupled inductor is composed of the magnetizing current (i_{Lm}) and the primary induced current (i_1). The secondary current (i_{L2}) is formed by the primary induced current (i_1) through the ideal transformer, and its value is related to the turns ratio (n). In addition, the conductive voltage drops of the switch (Q) and the diodes $(D_O, D_1,$ and $D_2)$ are neglected to simplify circuit analyses.

A. Operation Stages

1) Mode 1 $(t_0 - t_1)$ [Fig. 3(a)]: In this mode, the switch (Q) was turned on for a span. Because the magnetizing inductor (L_m) is charged by the input voltage source (V_S), the magnetizing current (i_{Lm}) increases gradually in an approximately linear way. The secondary voltage (v_{L2}) and the clamped capacitor voltage (v_{C1}) are connected in series to charge the high-voltage capacitor (C_2) through the switch (Q) and the rectifier diode (D_2). Thus, the magnitude of the secondary current (i_{L2}) is decreased since the high-voltage capacitor voltage (v_{C2}) is increased gradually. Since the primary current (i_{L1}) is the summation of the complementary currents $(i_{Lm}$ and $i_1)$, the current curve of i_{L1} is similar to a square wave. For the same reason, the switch current (i_{DS}) is also close to a square curve because the switch current (i_{DS}) is equal to the current summation of i_1, i_{Lm} and i_{L2}. The square primary current (i_{L1}) will result in lower copper loss in the coupled inductor, and the conduction loss of the switch also can be alleviated by the square switch current (i_{DS}).

2) Mode 2 $(t_1 - t_2)$ [Fig. 3(b)]: At the time $t = t_1$, the switch (Q) is turned off. At this time, the primary and secondary currents $(i_{L1}$ and $i_{L2})$ of the coupled inductor start to charge the parasitic capacitor of the switch. After the switch voltage (v_{DS}) is higher than the clamped capacitor voltage (v_{C1}), the clamped diode (D_1) conducts/transmits the energy of the primary-side leakage inductor (L_k) into the clamped capacitor (C_1). Moreover, the secondary current (i_{L2}) has to proceed continuously by way of the clamped diode (D_1) and rectifier diode (D_2) for releasing the energy of the secondary-side leakage inductor into the high-voltage capacitor (C_2). In this study, the clamped capacitor (C_1) is assumed to be large enough, with a favorable high-frequency response, so that its voltage (v_{C1}) can be viewed as a stable dc value with low ripple for clamping the maximum value of the switch voltage. In addition, the clamped diode (D_1) should be a fast conductive device and its voltage rating is the same as the switch (Q). Thus, the Schottky diode with low consumptive power and conductive voltage may be the better choice.
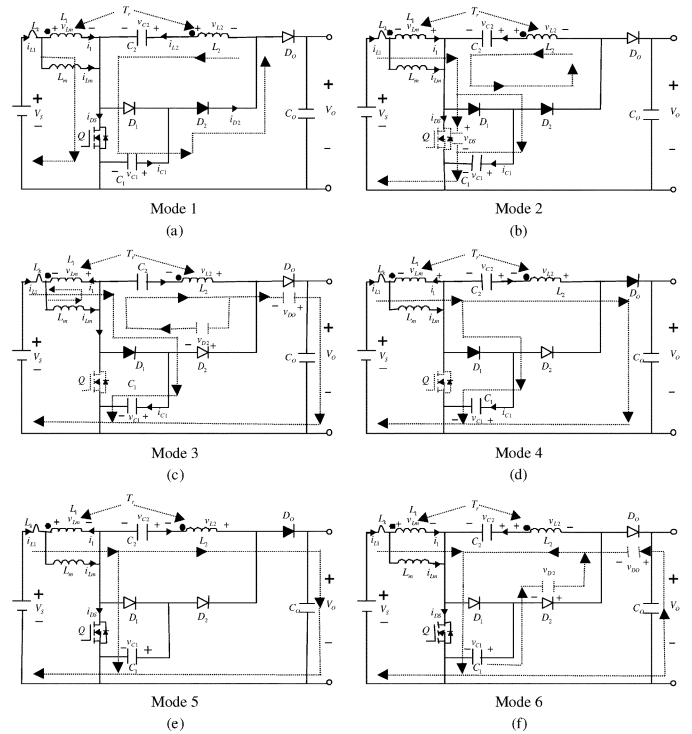

Fig. 3. Topological modes: (a) Mode 1 $[t_0-t_1]$, (b) Mode 2 $[t_1-t_2]$, (c) Mode 3 $[t_2-t_3]$, (d) Mode 4 $[t_3-t_4]$, (e) Mode 5 $[t_4-t_5]$, and (f) Mode 6 $[t_5-t_0]$.

3) Mode 3 $(t_2 - t_3)$ [Fig. 3(c)]: After releasing the leakage energy from the secondary side of the coupled inductor, the secondary current (i_{L2}) returns to zero at time $t = t_2$. Immediately, the secondary current (i_{L2}) is induced, in reverse, by the energy of the magnetizing inductor (L_m) through the ideal transformer. At the same time, the secondary current (i_{L2}) provides the reverse recovery current for the rectifier diode (D_2) to build its reverse-biased voltage (v_{D2}). This voltage (v_{D2}) will force the reverse parasitic voltage (v_{DO}) of the output diode (D_O) to decay to zero gradually. Because the current summation of the rectifier diode (D_2) and the output diode (D_O) is equal to the secondary current (i_{L2}), and the change rate of i_{L2} is limited by the leakage inductor in the secondary side of the coupled inductor, the reverse recovery and forward conductive currents of the diodes $(D_2$ and $D_O)$ are small. Moreover, they also have voltage clamped characteristics since the voltage summation of the rectifier diode (D_2) and the output diode (D_O) is equal to the output voltage (V_O) minus the clamped capacitor voltage (v_{C1}). If the output voltage is smaller than 200 V, the Schottky diodes can be adopted.

4) Mode 4 $(t_3 - t_4)$ [Fig. 3(d)]: At time $t = t_3$, the reverse parasitic voltage (v_{DO}) of the output diode (D_O) decays to zero and starts to conduct, and the rectifier diode (D_2) is cut off. At this time, the series voltages of $\mathrm{V}_S, v_{Lk}, v_{Lm}, v_{C2}$, and v_{L2} charges the output capacitor (C_O) and supplies the output load (R_O) by way of low current type. According to the conservation law of magnetic energy, it still supplies currents in the primary and secondary sides of the coupled inductor persistently after the entire consumption of the leakage inductor energy. The primary current (i_{L1}) charges the clamped capacitor (C_1) and passes through the secondary side of the coupled inductor, and

the secondary current (i_{L2}) delivers to the output terminal. In the middle stage of this mode, the high-voltage capacitor (C_2) is discharged and its voltage (v_{C2}) has a "descended sustainability." Moreover, the clamped capacitor voltage (v_{C1}) is increased by electrifying it for a long time, and the primary current (i_{L1}) is equal to the secondary current (i_{L2}) when the clamped diode (D_1) is reverse-biased.

5) Mode 5 $(t_4 - t_5)$ [Fig. 3(e)]: Since the clamped diode (D_1) is a low-voltage Schottky diode, it will be cut off promptly without reverse-recovery current when the switch (Q) is turned on at time $t = t_4$. Because the raising rate of the primary current (i_{L1}) is limited by the primary-side leakage inductor (L_k), and the secondary current (i_{L2}) needs time to decay to zero, these two currents depend on each other. Because it cannot derive any current from these three paths including the primary-side circuit, secondary-side circuit, and passive regenerative snubber circuit, the switch (Q) is turned on under zero-current-switching (ZCS) and this soft switching property is helpful for alleviating the switching loss. In this mode, the circuit current flow is still directed to the output terminal, but its magnitude decreases gradually.

6) Mode 6 $(t_5 - t_0)$ [Fig. 3(f)]: After releasing the leakage energy, the secondary current (i_{L2}) decays to zero at time $t = t_5$ and starts to pass through the switch (Q) inversely. At the same time, the output current provides the reverse recovery current for the output diode (D_O) to build its reverse-biased voltage (v_{DO}), and the secondary current (i_{L2}) leads the rectifier diode (D_2) to be forward-biased. When the rectifier diode (D_2) is conducted and the output diode (D_O) is cut off $(t = t_0)$, it begins the next switching cycle and repeats the operation in mode 1.

Remark 1: Presently, a ZCS magnetic integrated forward converter has received more attention [19], [20] due to the possible features of voltage stresses depending on the output voltage, wide voltage output range, and voltage isolation capability, the duty may be free-adopted in order to optimize the transistor profit factor, there is no capacitor inserted in the main path of power, or the output filter capacitor current is not pulsating. Although this ZCS forward converter has several advantages, it presents the following drawbacks. The common circuit topology is too complicated for practical implementation. Moreover, the voltage gain of the ZCS forward converter is limited by the turns ratio of the transformer. Generally speaking, high-efficiency, high step-up dc–dc converters for tenfold voltage gain applications have the common feature of no isolation [10].

B. Formula Derivation

When the switch (Q) is turned on, the voltages across the magnetizing inductor (L_m) can be denoted via (2) as

$$v_{Lm} = kV_S. \tag{3}$$

Moreover, the voltage across the secondary winding of the ideal transformer can be represented via (3) as

$$v_{L2} = nv_{Lm} = nkV_S. \tag{4}$$

Because the series voltages of v_{L2} and v_{C1} charge the high-voltage capacitor (C_2), the voltage across C_2 can be described via (4) as

$$v_{C2} = nkV_S + v_{C1}. \tag{5}$$

When the switch (Q) is turned off, the current of the leakage inductor (L_k) in the primary side of the coupled inductor flows persistently through the clamped capacitor (C_1) until the secondary current (i_{L2}) reacts upon the energy from the magnetizing inductor (L_m). Due to the concept of the zero average voltage across the leakage inductor (L_k) over one period [10], the required cycle to release the energy of the leakage inductor (L_k) can be denoted as

$$D_L = t_L/T_S = 2(1 - D)/(n + 1), \quad t_L = t_3 - t_1 \tag{6}$$

where T_S is the switching period, D is the duty cycle of the switch (Q), and t_L is the time from mode 2 to mode 3. Moreover, the voltages of v_{Lk} and v_{Lm} are given as

$$v_{Lk} = \frac{D(n + 1)(1 - k)}{2(1 - D)}V_S \tag{7}$$

$$v_{Lm} = DkV_S/(1 - D) \tag{8}$$

therefore, the clamped capacitor voltage (v_{C1}) can be represented via (7) and (8) as

$$v_{C1} = v_{Lk} + v_{Lm} + V_S$$
$$= \frac{V_S}{1 - D} + \frac{D(1 - k)(n - 1)}{2(1 - D)}V_S = v_{DS}. \tag{9}$$

Note, that the voltage of v_{C1} is equal to the switch voltage (v_{DS}). According to (8) and (9), the voltages of v_{C2} and v_{L2} can be rewritten as

$$v_{C2} = \left[nk + \frac{2 + D(1 - k)(n - 1)}{2(1 - D)}\right]V_S \tag{10}$$

$$v_{L2} = nv_{Lm} = DknV_S/(1 - D). \tag{11}$$

In the meantime, the voltages of v_{C1}, v_{C2}, and v_{L2} charge the output capacitor (C_O) and output load (R_O); therefore, the output voltage (V_O) can be calculated as

$$V_O = v_{C1} + v_{C2} + v_{L2}$$
$$= \frac{2 + nk}{1 - D}V_S + \frac{D(1 - k)(n - 1)}{1 - D}V_S. \tag{12}$$

As a result, the voltage gain of the proposed high step-up converter can be represented as

$$G_V = \frac{V_O}{V_S} = \frac{2 + nk}{1 - D} + \frac{D(1 - k)(n - 1)}{1 - D}. \tag{13}$$

Substituting $k = 1$ and $n = 1, 2, 4, 6, 8$ into (13), the curve of the voltage gain (G_V) with respect to the duty cycle (D) is depicted in Fig. 4(a), where the line labeled with a star denotes the voltage gain curve of the newly designed converter and the real line represents the one in [10]. As can be seen from Fig. 4(a), the voltage gain of the proposed high step-up converter is higher than a coupled-inductor-based converter in [10], especially in
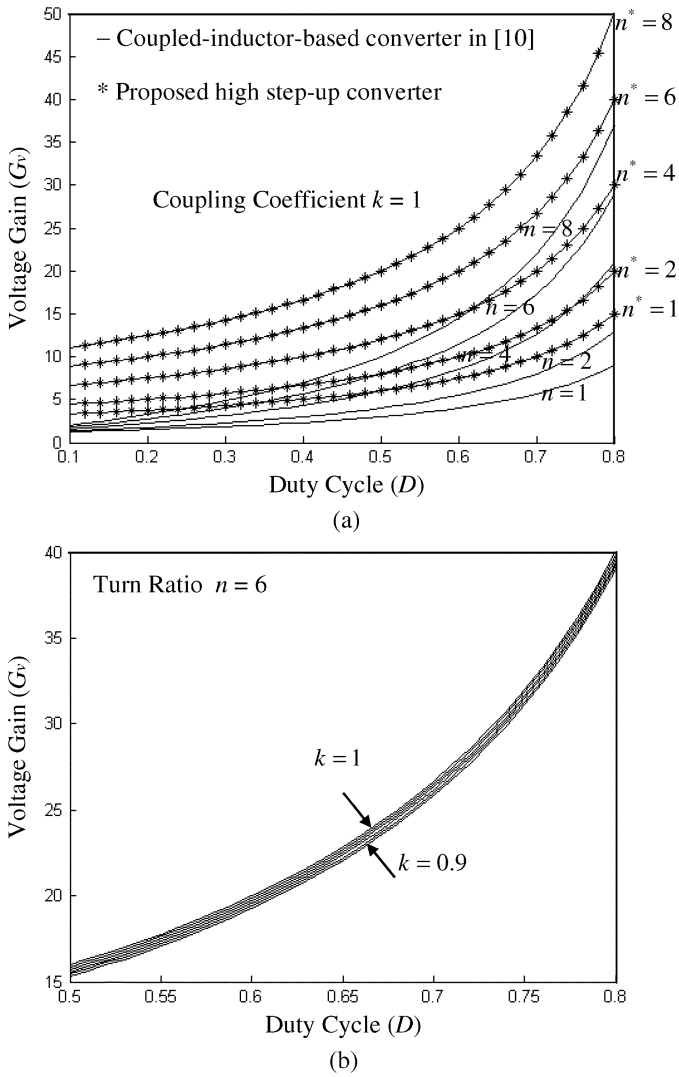
Fig. 4. Voltage gain curve: (a) coupling coefficient $k = 1$ and (b) turn ratio $n = 6$.

the smaller duty cycle. For example, one can obtain $G_V = 40$ if the values of $k = 1, n = 6$, and $D = 0.8$ are selected. It can verify that the switch duty cycle in the proposed converter can be operated under a wide range. Moreover, the voltage gain curve by substituting $k = 0.9–1$ and $n = 6$ into (13) is depicted in Fig. 4(b). By observing this figure, the voltage gain (G_V) is less sensitive to the coupling coefficient, k. For simplicity, the coupling coefficient (k) is set at one, then (9) and (13) can be rewritten as

$$v_{C1} = V_S/(1 - D) = v_{DS} \tag{14}$$

$$G_V = \frac{V_O}{V_S} = \frac{2 + n}{1 - D}. \tag{15}$$

If the value of $D = 0.5$ is selected, the voltage gain in (15) is two times the ones in [10] and [11]. According to (14) and (15), one can obtain

$$v_{DS} = V_O/(n + 2). \tag{16}$$

By analyzing (16), the switch voltage (v_{DS}) is not related to the input power source (V_S) and the switch duty cycle (D) if the
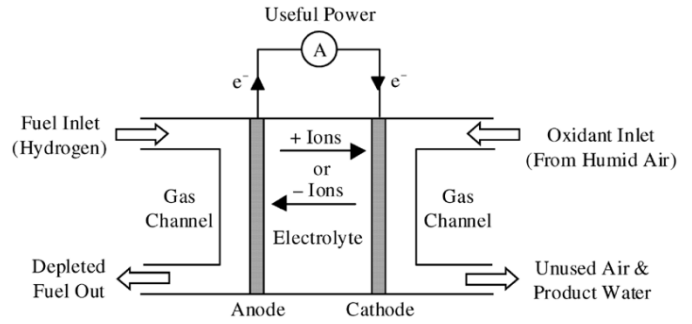

Fig. 5. Fuel cell basic configuration.

values of the output voltage (V_O) and the turns ratio (n) are fixed. Thus, it can ensure that the maximum sustainable voltage of the switch (Q) is constant. As long as the input voltage is not higher than the switch voltage-rated, the proposed high step-up converter can be applied well to low-voltage power sources even with large voltage variations, e.g., photovoltaic cells, wind generator, fuel cells, batteries, etc.

Fuel cell generation systems have been receiving more attention in the last years due to the advantages of their high efficiency, low aggression to the environment, no moving parts and superior reliability and durability. The basic fuel cell structure is illustrated in Fig. 5, [15], and the fuel cell operating principle is described briefly in the Appendix. Due to the electrochemical reaction, fuel cell has the power quality of low voltage and high current. However, the fuel cell stack with high output voltage is difficult to fabricate and it may be failure when any single cell is inactive. Besides, the output voltage is varied easily with respect to the load variations. In order to satisfy the requirement of high-voltage demand, a stable boost converter with high voltage gain and superior conversion efficiency is necessary in order to utilize the fuel cell energy more efficiently and satisfy the requirement of high-voltage demand in some applications. For examples, a travelling wave tube amplifier (TWTA) [1], a high intensity discharge (HID) lamp [21], the high-voltage dc bus of an uninterruptible power supply (UPS), etc. The validity of the proposed converter is verified by the following experimental results.

III. EXPERIMENTAL RESULTS

In order to verify the effectiveness of the designed topology, a PEMFC system and a traditional battery are utilized for low-voltage power sources in the proposed high step-up converter. The PEMFC system used in this study is the PowerPEMTM-PS250 manufactured by the Hpower Company. It is a dc power source with a 250-W dc nominal power rating. The system operates on ambient air and clean pressurized hydrogen fuel. The fuel cell system consists of a (40) cell stack of the PEM type, mechanical auxiliaries, and electronic control module.

In the experiment, the high step-up converter is designed initially to operate from the fuel cell variability dc input, $V_{IN} = 25–38$ V, to deliver a constant dc output, $V_O = 400$ V. Assume that the maximum value of the switch voltage is clamped at 50 V, the turns ratio $n = (V_O/v_{DS(max)}) - 2 = 6$ according to (16). From (15), the related duty cycle, $D = 0.8$, is reasonable in practical applications if the minimum input voltage is assumed

to be 10 V. In order to solve the problem of the fuel cell output voltage varied with the load variations, the proposed converter with dc voltage feedback control is utilized to ensure the system stability, and a PWM control IC TL494 is adopted to achieve this goal of feedback control. The prototype with the following specifications is designed in this section to illustrate the design procedure given in Section II.

Switching frequency

$f_S = 100$ kHz;

Coupled inductor

$L_1 = 13 \ \mu H; \quad L_2 = 470 \ \mu H; \quad N_1 : N_2 = 3{:}18;$

$k = 0.98; \quad EE{-}55$ core;

Capacitor

$C_{IN} = 3300 \ \mu F/50 \ V * 2; \quad C_1 = 5 \ \mu F/100 \ V;$

$C_2 = 6.8 \ \mu F/250 \ V; \quad C_O = 47 \ \mu F/450 \ V;$

Switch

Q: FQI90N08(80 V/71 A, $R_{DS(\,on)} = 16$ mΩ), I^2PAK;

Diode

D_1: Schottky diode STPS20H100CT,

TO$-$220AB (100 V/2 * 10 A);

D_2, D_O: SFA1606G, TO$-$220AB (400 V/16 A).

The experimental voltage and current responses of the proposed high step-up converter operating at 300 W-output power is depicted in Fig. 6. From Fig. 6(a), the switch voltage (v_{DS}) is clamped at 50 V which is much smaller than the output voltage, $V_O = 400$ V, and the curve of the switch current (i_{DS}) is similar to a square wave so that it can further reduce the conduction loss of the switch (Q). By observing Fig. 6(b) and (c), the primary current (i_{L1}) keeps about 20 A, thus, only a smaller core capacity is necessary for $L_1 = 13 \ \mu H$. According to Fig. 6(d)–(j), the reverse-recovery currents in all of the diodes (D_O, D_1, and D_2) can be alleviated effectively, and the voltages of the clamped capacitor (C_1) and the high-voltage capacitor (C_2) are close to constant values. Therefore, it can alleviate the reverse-recovery problem and exhibit the voltage-clamped effect for further raising the conversion efficiency. In order to examine the robust performance of the proposed converter scheme, the experimental result of output voltage (V_O) and output current (I_O) under the step load variation between light-load (20 W) and heavy-load (300 W) is depicted in Fig. 6(k). As can be seen from Fig. 6(k), the converter output voltage, $V_O = 400$ V, is insensitive to the load variations due to the utilization a small coupled-inductor and a closed-loop control, and the output voltage ripple is also slight, especially as a result of high switching frequency. For the sake of verifying the effectiveness of the proposed converter for different output powers, the experimental switch voltage and current responses at 32 W, 120 W, 210 W, 272 W, 332 W, and 372 W-output powers are given in Fig. 7. As can be seen from these results, it needs to raise the duty cycle (D) to keep a constant output voltage ($V_O = 400$ V) since the fuel cell voltage drops when the output power increases. Moreover, the
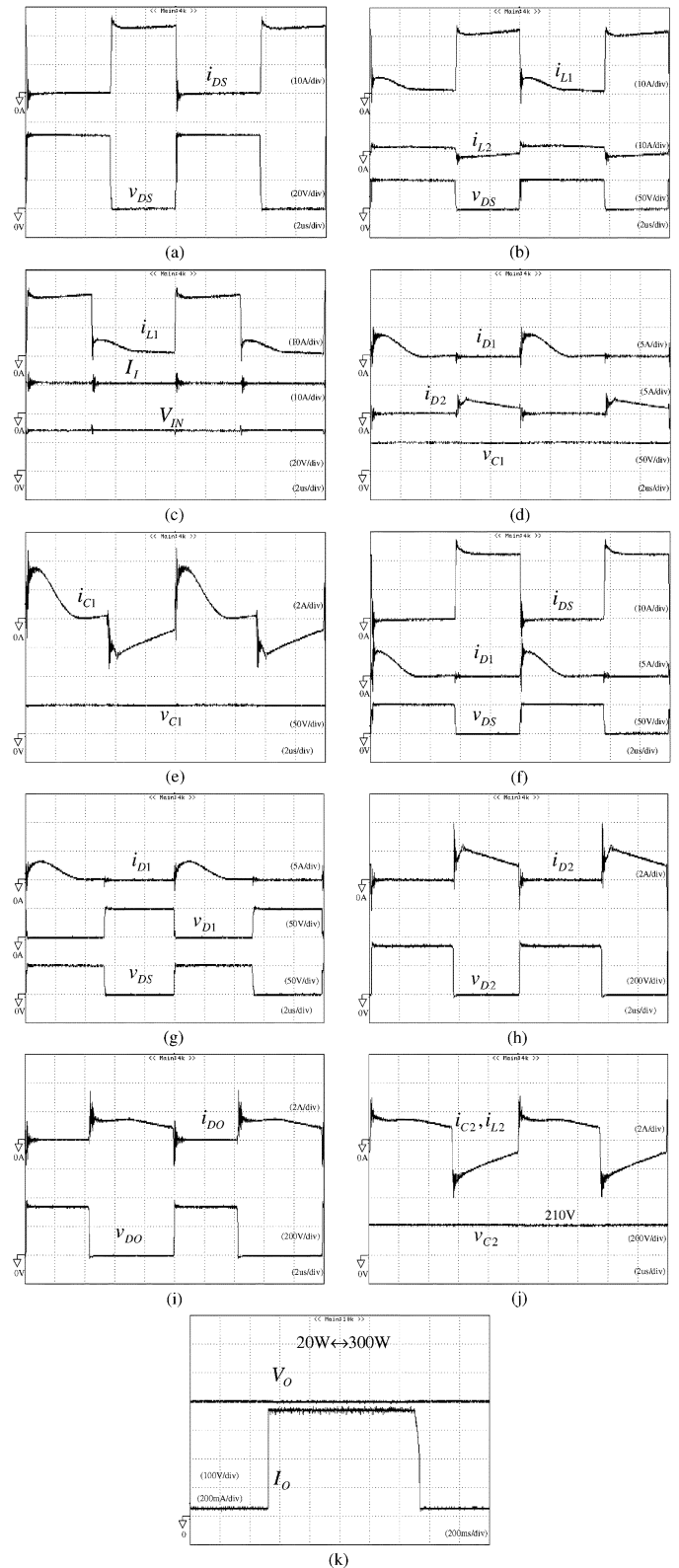

Fig. 6. Experimental voltage and current responses of high step-up converter for PEMFC with $P_O = 300$ W and $V_O = 400$ V.

switch voltage (v_{DS}) is still clamped at 50 V, and the curve of the switch current (i_{DS}) is also close to a square wave with low ripple. Note that, the oscillated switch voltage in Fig. 7(a) is caused by the resonance of the leakage inductance (L_k) and the switch parasitic capacitor at low power output [22]. It is
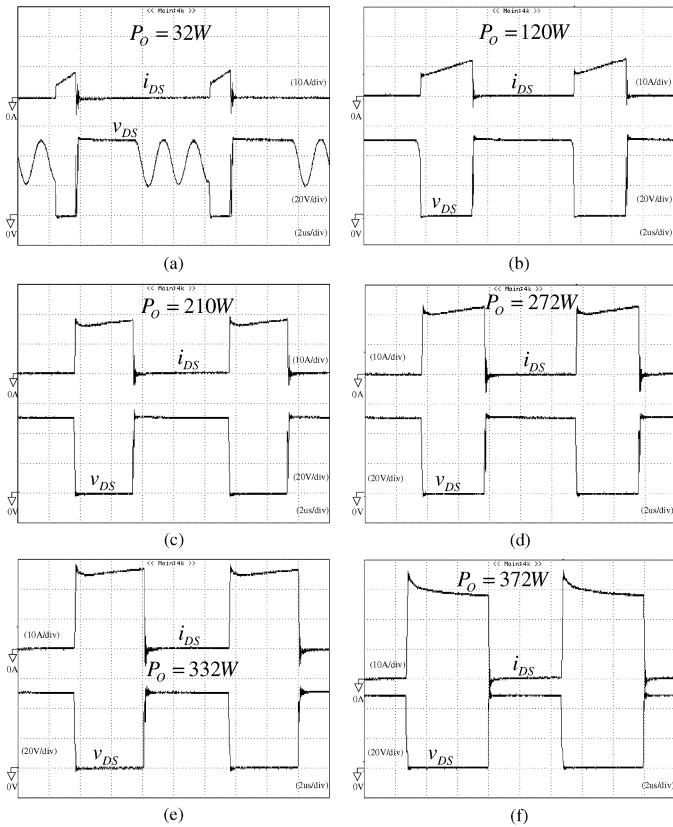
Fig. 7. Experimental switch voltage and current curves of high step-up converter for PEMFC with $V_O = 400$ V: (a) $P_O = 32$ W, (b) $P_O = 120$ W, (c) $P_O = 210$ W, (d) $P_O = 272$ W, (e) $P_O = 332$ W, and (f) $P_O = 372$ W.
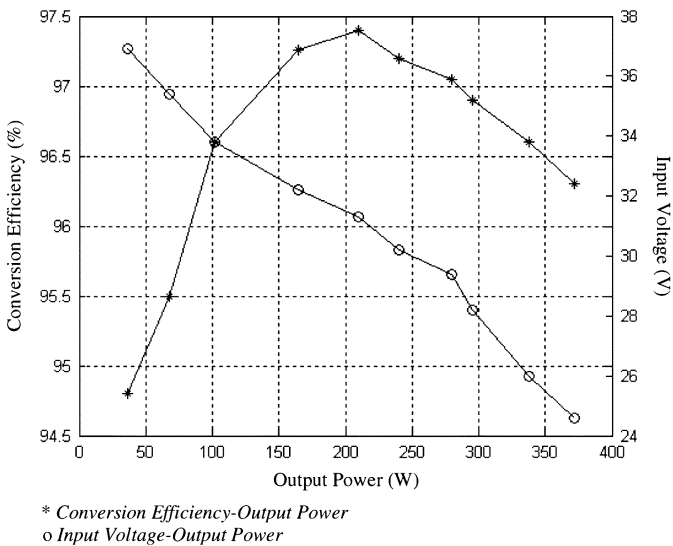

* Conversion Efficiency-Output Power
o Input Voltage-Output Power

Fig. 8. Conversion efficiency and fuel cell voltage for PEMFC with $V_O = 400$ V under different output powers.

Fig. 9. Experimental voltage and current responses of high step-up converter for 12 V-battery with $P_O = 210$ W and $V_O = 400$ V.

helpful to alleviate the switching loss in mode 5. Fig. 8 summarizes the experimental conversion efficiency of the proposed converter and fuel cell voltage under different output powers. From the experimental results, the output voltage of the fuel cell decreases as the output power increases, and it is varied easily with respect to the load variations. In order to solve this phenomenon, the proposed high step-up converter with
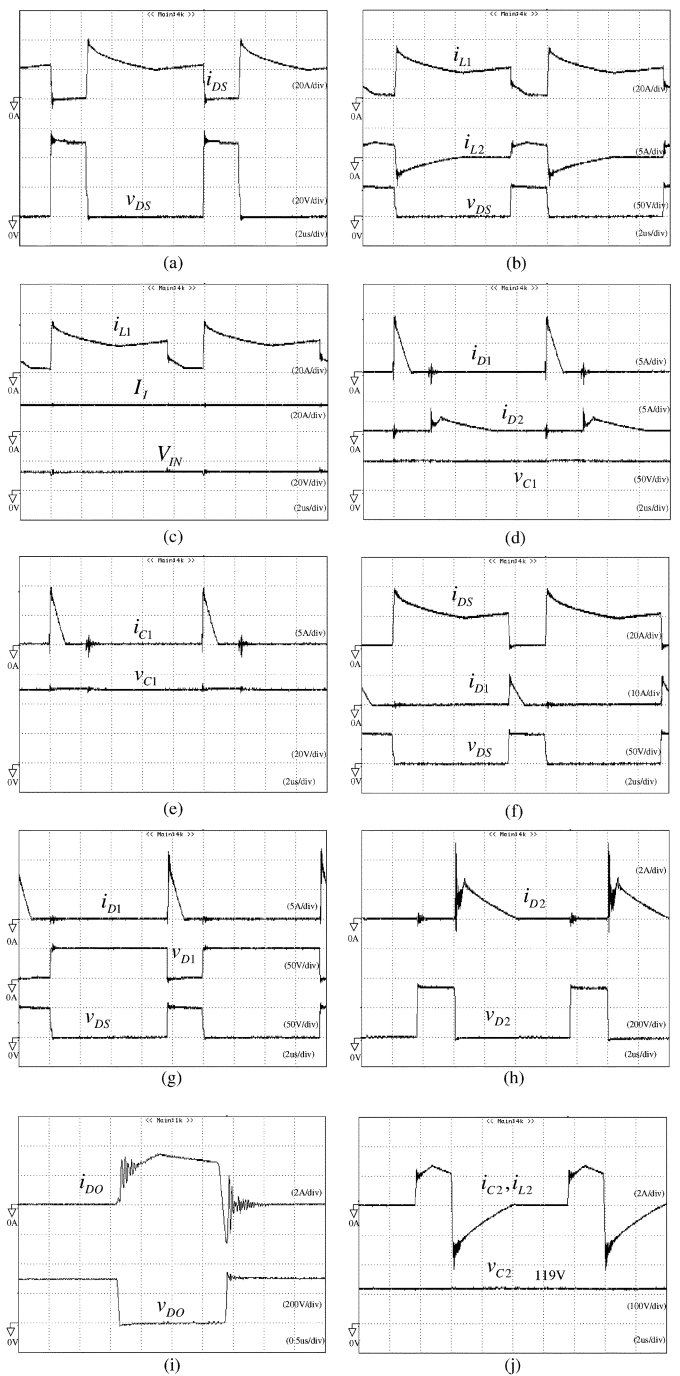
dc voltage feedback control is utilized in this study to ensure the system stability. In addition, the conversion efficiency at 40 W-output power is over 94.5% and the maximum efficiency is over 97% at 210 W-output power, which is comparatively higher than conventional converters.

In the following experimentation, a traditional battery is adopted for another low-voltage power source to further examine the characteristics of the high voltage gain and superior conversion efficiency of the proposed converter strategy. First, the high step-up converter is designed to operate from the battery dc input, $V_{IN} = 12$ V, to deliver a constant dc output,
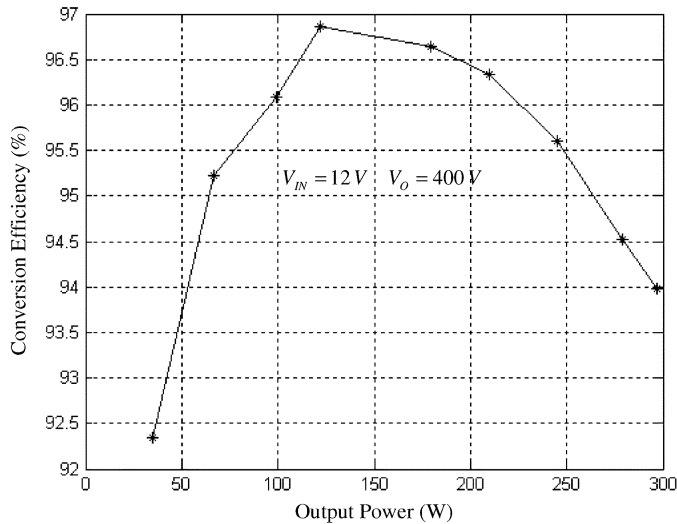
Fig. 10. Conversion efficiency for 12 V-battery with $V_O = 400$ V under different output powers.

$V_O = 400$ V. The associated experimental voltage and current responses of the proposed high step-up converter operating at 210 W-output power is depicted in Fig. 9. These experimental results agree well with those obtained from PEMFC system given in Fig. 6. Compare these two figures, it also can achieve the voltage-clamped purpose even though the current ripples in Fig. 9 are slightly higher than the ones in Fig. 6. Thus, it can concluded that this converter still has favorable designed properties given in Section II under the condition of the voltage gain over thirty-three. Fig. 10 summarizes the experimental conversion efficiency of the proposed converter under different output powers. At this examined condition, the maximum efficiency over 96.5% is slightly smaller than the one in Fig. 8 because its voltage gain is $G_V = 400/12$. Immediately, the experimental switch voltage and current responses at 12 V, 16 V, 20 V, 24 V, 26 V, and 30 V-input voltages for 400 V-output voltage and 100 W-output power are given in Fig. 11 for exhibiting the performance of the proposed converter for different input voltages. Moreover, the related conversion efficiency of the proposed converter under different input voltages is summarized in Fig. 12. As can been seen from these results, the conversion efficiency is near to 98% at 25 V-input voltage ($G_V = 16$), and the conversion efficiency is 94.5% at the minimum 8 V-input voltage ($G_V = 50$). Consequently, the designed object of high-efficiency, high step-up and voltage-clamped characteristics can be achieved perfectly.

The experimental inductor current and switch voltage curves of a coupled-inductor converter in [10] and the proposed converter are depicted in Fig. 13(a) and (b), where the operation condition is summarized as $V_{IN} = 24$ V, $V_O = 200$ V, $P_O = 800$ W, and $f_S = 100$ kHz. Moreover, the coupled inductors are designed as $L_1 = 11.3\ \mu$H, $L_2 = 290\ \mu$H, $N_1 : N_2 = 3:15$ in the coupled-inductor converter of [10], and $L_1 = 11.3\ \mu$H, $L_2 = 45\ \mu$H, $N_1 : N_2 = 3:6$ in the proposed converter under the EE-55 core with the same air gap, respectively. Due to the continuous inductor current conduction, the peak current and voltage stresses of the proposed converter are smaller than the one in [10]. Consequently, the proposed converter can adopt
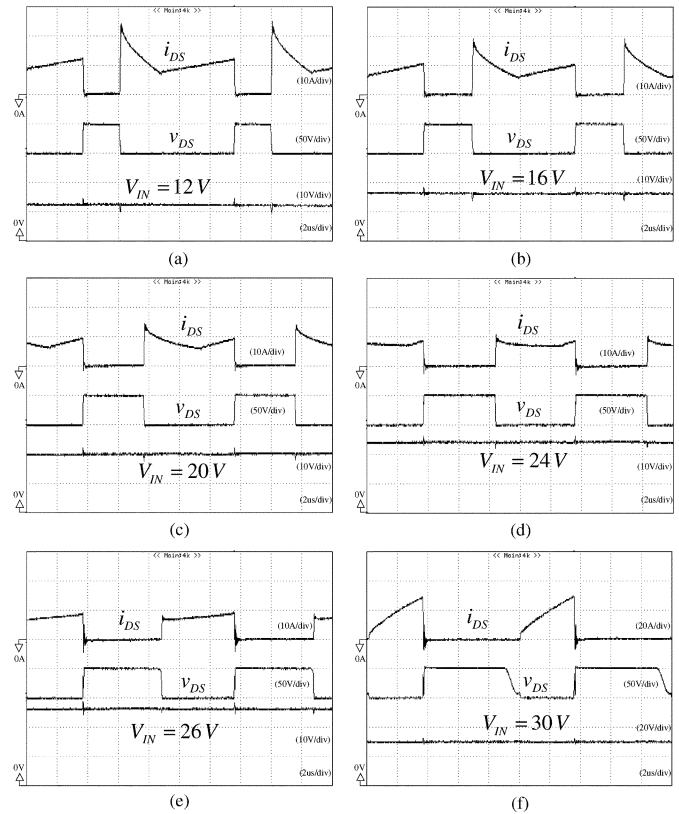

Fig. 11. Experimental switch voltage and current curves of high step-up converter for battery with $P_O = 100$ W and $V_O = 400$ V: (a) $V_{IN} = 12$ V, (b) $V_{IN} = 16$ V, (c) $V_{IN} = 20$ V, (d) $V_{IN} = 24$ V, (e) $V_{IN} = 26$ V, and (f) $V_{IN} = 30$ V.
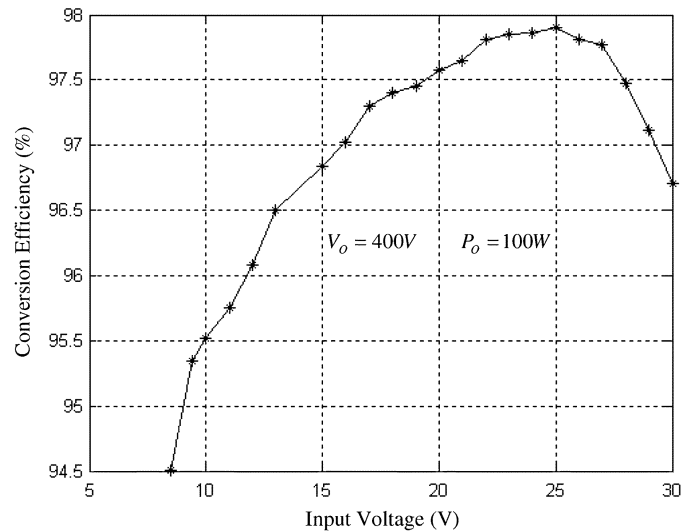

Fig. 12. Conversion efficiency for battery with $P_O = 100$ W and $V_O = 400$ V under different input voltages.

a 75 V-rated voltage switch with lower conduction losses for $i^2 R_{DS(on)}$ and the smaller inductor current will result in the utilization of a lower volume of the magnetic core.

In order to examine the coupled-inductor capability, the experimental inductor current and switch voltage curves of the proposed converter under the condition of $V_{IN} = 24$ V, $V_O = 200$ V, and $P_O = 1$ kW is depicted in Fig. 14. As a result,
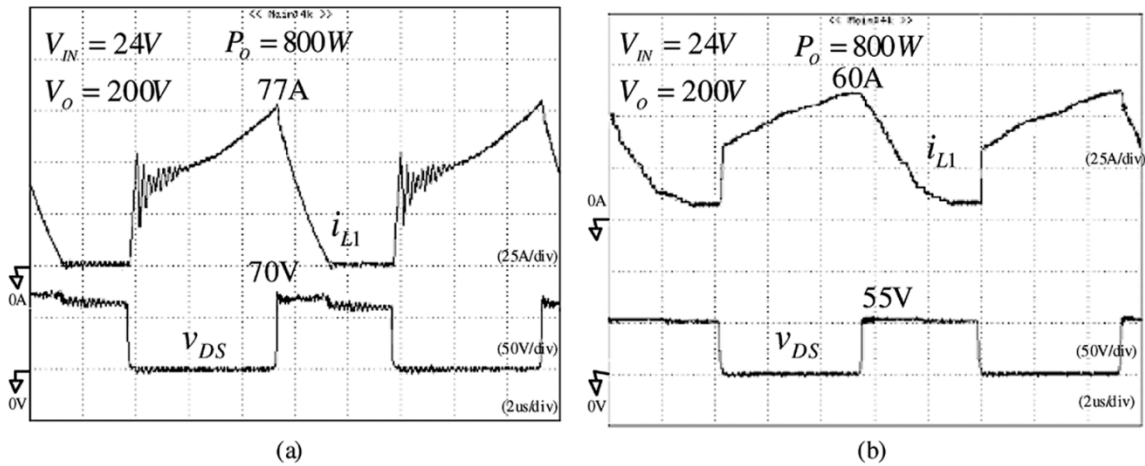
Fig. 13. Experimental inductor current and switch voltage curves of coupled-inductor converter in [10] and high step-up converter with $V_{IN} = 24$ V, $V_O = 200$ V and $P_O = 800$ W.
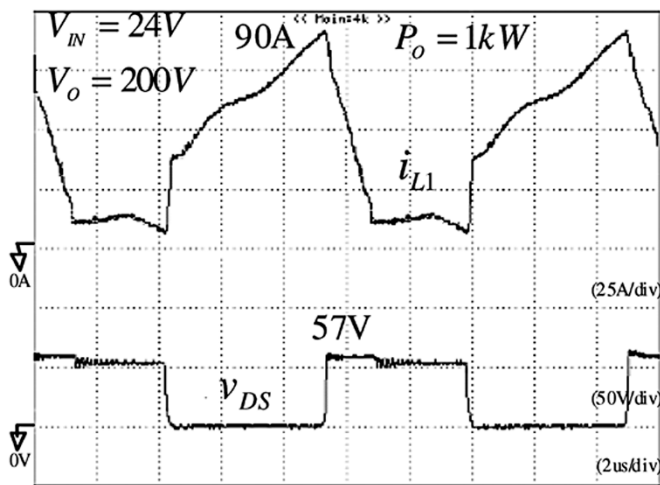

Fig. 14. Experimental inductor current and switch voltage curves of high step-up converter with $V_{IN} = 24$ V, $V_O = 200$ V and $P_O = 1$ kW.
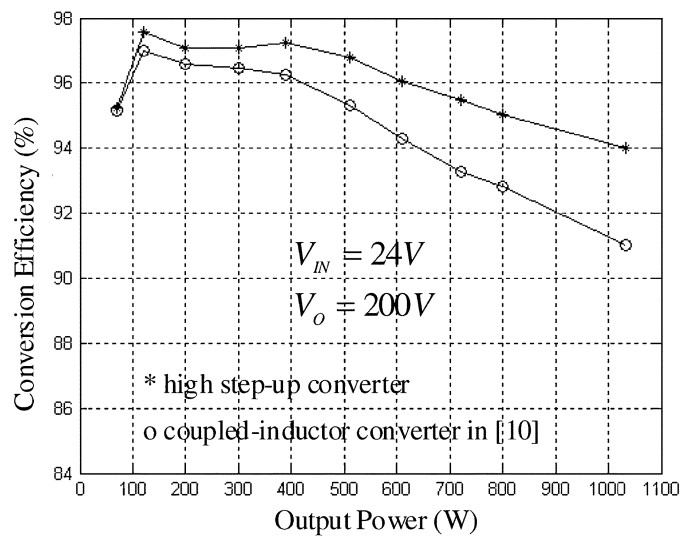

Fig. 15. Conversion efficiency of coupled-inductor converter in [10] and high step-up converter for 24 V-battery with $V_O = 200$ V under different output powers.

the proposed converter with the same size of the coupled inductor can be operated over 1 kW power. Note that, the circulating current is only induced by the current $i_{L2} = (i_{L1} - i_{Lm})/n = i_1/n$ during mode 1 and its value is smaller relatively than the switch current i_{DS} as shown in Fig. 6(b). Therefore, the extremely small circulating current involved in soft-switching snubber operation is not enough to result in the burden of the coupled inductor. Though all the power is transferred through a high-voltage capacitor (C_2) by a nearly square wave current as shown in Fig. 6(j), this current $i_{C2} = i_{L2}$ is relatively small and its change is limited by the leakage inductor of the coupled indictor. As can be seen from Fig. 14, the proposed converter is suitable for a higher power application. To survey other topologies with capacitor inserted in the main power (e.g., the magnetic integrated Cuk converter, the SEPIC and the dual SEPIC), the capacitor usually connects in series with the low-voltage side. As a result, it will result in a high capacitor current so that these previous schemes have inherent drawbacks for high power applications.

The conversion efficiency of a coupled-inductor converter in [10] and the proposed converter for a 24 V-battery with $V_O =$

200 V under different output powers is depicted in Fig. 15. In Fig. 15, the related semiconductor profit factors are 5.8% (IRFPS3810) and 6.4% (IRFP2907), respectively, where the definition of the semiconductor profit factor is the rate between the converter power output (1 kW) versus total semiconductor sizing power. From this comparison, the proposed high step-up converter indeed yields superior conversion efficiency over that of the coupled-inductor converter in [10] under nearly the same semiconductor profit factors. Note, that the snubber current can be efficiently recycled by the series high-voltage capacitor, and is then discharged directly to the output by the secondary coupled winding. Although it will increase the main switch current, the switch conduction loss caused by the smaller inductor current (i_{L2}) can be nearly ignored.

IV. CONCLUSION

This study has successfully developed a high step-up converter with a coupled-inductor, and this converter has been ap-

plied well for a PEMFC system and a traditional battery. According to the experimental results, the maximum efficiency was measured to be over 96.5%, which is comparatively higher than conventional converters with the same voltage gain. The efficiency of this circuit can be further optimized by using a lower-voltage-rated switch with low $R_{\text{DS(on)}}$ and building the circuit more compactly via a PCB layout. The newly designed converter circuit has the following features. 1) The voltage gain can be greatly heightened due to the utilization of a coupled inductor with a lower turns ratio. 2) The stray energy can be recycled by a passive regenerative snubber to contribute toward both the step-up and a voltage-clamped object so that the circuit layout is easy in practical applications. 3) The switch voltage stress is not related to the input voltage, thus, it is more suitable for a dc power conversion mechanism with high voltage variation range. 4) The diode short-circuit and reverse-recovery problems can be solved because of all the diodes possessing voltage clamped properties. 5) The copper loss in the magnetic core can be greatly reduced and the EMI problem can be alleviated easily. 6) The voltage drift problem of the power source under the load variations can be coped with through the utilization of a small coupled-inductor and a closed-loop control. This high-efficiency converter topology provides designers with an alternative choice to convert renewable energy efficiently, and it also can be extended easily to other power conversion systems for satisfying high-voltage demands.
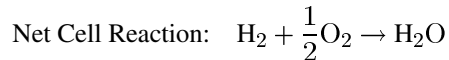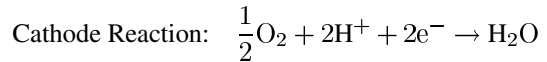
APPENDIX

A. Fuel Cell Operating Principle

The basic fuel cell concept involves converting chemical energy directly into electrical energy. It produces electricity by electrochemically combining fuel (hydrogen) and oxidant (oxygen from the air) gases through electrodes and across an ion-conducting electrolyte. The fuel cell is composed of two electrodes, an anode, cathode, the catalyst, and an electrolyte [15]. The main function of the electrode is to bring about a reaction between the reactant and the electrolyte. The anode, used as the negative post in the fuel cell, disperses the hydrogen gas equally over the entire catalyst surface and conducts the electrons for use as power in an external circuit. The cathode, used as the positive post in the fuel cell, distributes the oxygen fed to it onto the catalyst surface and conducts the electrons back from the external circuit. The catalyst is a special material used to facilitate the oxygen and hydrogen reaction.

According to the chemical characteristics of the electrolyte used as the ion conductor in the cells, the most promising types are classified as 1) proton exchange membrane fuel cell (PEMFC) and direct methanol fuel cell (DMFC), which use a polymer membrane as the electrolyte. 2) Phosphoric acid fuel cell (PAFC), which uses pure phosphoric acid as the electrolyte. 3) Molten carbonate fuel cell (MCFC), which uses a molten mixture, sodium, and potassium carbonates as the electrolyte. 4) Solid oxide fuel cell (SOFC), which uses a ceramic material as the electrolyte [16].

The PEMFC is one of the most promising fuel cell types, and is often considered a potential replacement for the internal combustion engine in transportation applications [16]. The PEMFC consists of porous carbon electrodes bound to a thin sulphonated polymer membrane. The anode, cathode, and net cell reactions of the PEMFC can be represented as

Anode Reaction: $\quad H_2 \rightarrow 2H^+ + 2e^-$

Cathode Reaction: $\quad \dfrac{1}{2}O_2 + 2H^+ + 2e^- \rightarrow H_2O$

Net Cell Reaction: $\quad H_2 + \dfrac{1}{2}O_2 \rightarrow H_2O$

where the mobile ion is H^+. The membrane electrode assembly (MEA) is sandwiched between two collector plates that provide an electrical path from the electrodes to the external circuit. Flow channels cut into the collector plates distribute reactant gases over the surface of the electrodes. Individual cells consisting of collector plates and MEAs are assembled in series to form a fuel cell stack.

ACKNOWLEDGMENT

REFERENCES

[1] I. Barbi and R. Gules, "Isolated dc–dc converters with high-output voltage for TWTA telecommunication satellite applications," *IEEE Trans. Power Electron.*, vol. 18, no. 4, pp. 975–984, Jul. 2003.

[2] O. Abutbul, A. Gherlitz, Y. Berkovich, and A. Ioinovici, "Step-up switching-mode converter with high voltage gain using a switched-capacitor circuit," *IEEE Trans. Circuit Syst. I*, vol. 50, no. 8, pp. 1098–1102, Aug. 2003.

[3] K. C. Tseng and T. J. Liang, "Novel high-efficiency step-up converter," *Proc. Inst. Elect. Eng.*, vol. 151, pp. 182–190, 2004.

[4] N. Mohan, T. M. Undeland, and W. P. Robbins, *Power Electronics: Converters, Applications, and Design*. New York: Wiley, 1995.

[5] M. M. Jovanovic and Y. Jang, "A new soft-switched boost converter with isolated active snubber," *IEEE Trans. Ind. Appl.*, vol. 35, no. Mar./Apr., pp. 496–502, 1999.

[6] C. M. C. Duarte and I. Barbi, "An improved family of ZVS-PWM active-clamping DC-to-DC converters," *IEEE Trans. Power Electron.*, vol. 17, no. 1, pp. 1–7, Jan. 2002.

[7] E. S. da Silva, L. dos Reis Barbosa, J. B. Vieira, L. C. de Freitas, and V. J. Farias, "An improved boost PWM soft-single-switched converter with low voltage and current stresses," *IEEE Trans. Ind. Electron.*, vol. 48, no. 6, pp. 1174–1179, Dec. 2001.

[8] K. Hirachi, M. Yamanaka, K. Kajiyama, and S. Isokane, "Circuit configuration of bidirectional DC/DC converter specific for small scale load leveling system," in *Proc. IEE Power Conversion Conf.*, 2002, pp. 603–609.

[9] C. W. Roh, S. H. Han, and M. J. Youn, "Dual coupled inductor fed isolated boost converter for low input voltage applications," *Electron. Lett.*, vol. 35, pp. 1791–1792, 1999.

[10] Q. Zhao and F. C. Lee, "High-efficiency, high step-up dc–dc converters," *IEEE Trans. Power Electron.*, vol. 18, no. 1, pp. 65–73, Jan. 2003.

[11] K. C. Tseng and T. J. Liang, "Novel high-efficiency step-up converter," *Proc. Inst. Elect. Eng.*, vol. 151, pp. 182–190, 2004.

[12] R. Kyoungsoo and S. Rahman, "Two-loop controller for maximizing performance of a grid-connected photovoltaic-fuel cell hybrid power plant," *IEEE Trans. Energy Conv.*, vol. 13, no. 3, pp. 276–281, Sep. 1998.

[13] M. D. Lukas, K. Y. Lee, and H. Ghezel-Ayagh, "Development of a stack simulation model for control study on direct reforming molten carbonate fuel cell power plant," *IEEE Trans. Energy Conv.*, vol. 14, no. 4, pp. 1651–1657, Dec. 1999.

[14] M. D. Lukas, K. Y. Lee, and H. Ghezel-Ayagh, "An explicit dynamic model for direct reforming carbonate fuel cell stack," *IEEE Trans. Energy Conv.*, vol. 16, no. 3, pp. 289–295, Sep. 2001.

[15] A. B. Stambouli and E. Traversa, "Fuel cells, an alternative to standard sources of energy," *Renewable Sustainable Energy Rev.*, vol. 6, pp. 297–306, 2002.

[16] M. W. Ellis, M. R. Von Spakovsky, and D. J. Nelson, "Fuel cell systems: Efficient, flexible energy conversion for the 21st century," *Proc. IEEE*, vol. 89, no. 12, pp. 1808–1818, Dec. 2001.

[17] J. M. Correa, F. A. Farret, J. R. Gomes, and M. G. Simoes, "Simulation of fuel-cell stacks using a computer-controlled power rectifier with the purposes of actual high-power injection applications," *IEEE Trans. Ind. Applicat.*, vol. 39, no. 4, pp. 1136–1142, Jul./Aug. 2003.

[18] K. Green and J. C. Wilson, "Future power sources for mobile communications," *Proc. Inst. Elect. Eng.*, pp. 43–47, 2001.

[19] H. Muraoka and M. Nakaoka, "High-frequency PWM forward converter with auxiliary active clamped capacitor for low voltage high current operation," in *Proc. IEEE Power Electronics Specialists Conf.*, vol. 3, 2001, pp. 1523–1528.

[20] E. S. da Silva, E. A. A. Coelho, L. C. de Freitas, J. B. Vieira, and V. J. Farias, "A soft-single-switched forward converter with low stresses and two derived structures," *IEEE Trans. Power Electron.*, vol. 19, no. 2, pp. 388–395, Mar. 2004.

[21] J. E. Harry and D. W. Hoare, "Electronic power supplies for high-density discharge (HID) lamps," *Proc. Inst. Elect. Eng.*, pp. 203–206, 2000.

[22] D. C. Lu, D. K. W. Cheng, and Y. S. Lee, "A single-switch continuous-conduction-mode boost converter with reduced reverse-recovery and switching losses," *IEEE Trans. Ind. Electron.*, vol. 50, no. 4, pp. 767–776, Aug. 2003.

Rou-Yong Duan was born in Nantou, Taiwan, R.O.C., in 1965. He received the B.S. degree from National Kaohsiung University of Applied Sciences, Kaohsiung, Taiwan, in 1986, the M.S. degree from Chung Yuan Christian University, Chung Li, Taiwan, in 1998, and the Ph.D. degree from Yuan Ze University, Chung Li, in 2004, all in electrical engineering.

Since August 2004, he has been an Assistant Professor with the Department of Industrial Safety and Health, Hung Kuang University, Tai-Chung, Taiwan. His research interests include motor servo drives, resonant theory, power electronics, and renewable energy.

Rong-Jong Wai (M'00) was born in Tainan, Taiwan, R.O.C., in 1974. He received the B.S. degree in electrical engineering and the Ph.D. degree in electronic engineering from Chung Yuan Christian University, Chung Li, Taiwan, R.O.C., in 1996 and 1999, respectively.

Since 1999, he has been with the Department of Electrical Engineering, Yuan Ze University, Chung Li, Taiwan, R.O.C., where he is currently an Associate Professor. He is also the Director of the Electric Control and System Engineering Laboratory at Yuan Ze University, and the Energy Conversion and Power Conditioning Laboratory at the Fuel Cell Center. He is a chapter-author of *Intelligent Adaptive Control: Industrial Applications in the Applied Computational Intelligence Set* (Boca Raton, FL: CRC Press, 1998) and the co-author of *Drive and Intelligent Control of Ultrasonic Motor* (Tai-Chung, Taiwan, R.O.C.: Tsang-Hai, 1999), *Electric Control* (Tai-chung, Taiwan, R.O.C.: Tsang-Hai, 2002) and *Fuel Cell: New Generation Energy* (Tai-chung, Taiwan, R.O.C.: Tsang-Hai, 2004). He has authored numerous published journal papers in the area of control system applications. His research interests include power electronics, motor servo drives, mechatronics, energy technology, and control theory applications.

Dr. Wai received the Excellent Research Award in 2000, the Wu Ta-You Medal and Young Researcher Award in 2003 from the National Science Council, R.O.C., the Outstanding Research Award in 2003 from the Yuan Ze University, R.O.C., the Excellent Young Electrical Engineering Award in 2004 from the Chinese Electrical Engineering Society, R.O.C, the Outstanding Professor Award in 2004 from the Far Eastern Y. Z. Hsu—Science and Technology Memorial Foundation, R.O.C., and the International Professional of the Year Award in 2005 from the International Biographical Center. He was listed in *Marquis Who's Who in Science and Engineering* in 2003 and also in *Leading Scientists of the World* in 2005.